JOM, Vol. 74, No. 11, 2022
https://doi.org/10.1007/s11837-022-05389-8

Tapping Gas from the Silicon Submerged Arc Furnace: An Industrial Measurement Campaign

VEGAR ANDERSEN ,[1,3] HEIKO GAERTNER,[2] SVEND GRÅDAHL,[2] MICHAL KSIAZEK,[2] KRISTIAN ETIENNE EINARSRUD,[1] and GABRIELLA TRANELL[1]

1.—Norwegian University of Science and Technology, Trondheim, Norway. 2.—SINTEF Industry, Trondheim, Norway. 3.—e-mail: vegar.andersen@ntnu.no

Producing high-silicon alloys in submerged arc furnaces (SAF) involves the generation of an intermediate process gas, consisting of silicon monoxide (SiO) and carbon monoxide (CO). Combustion of process gas from the taphole can be an environmental challenge. SiO gas burns to fine SiO_2 particles which can cause poor working conditions and fugitive particulate matter emissions. The high combustion energy of SiO and CO is a source of high heat load. It is also the source of thermal NO_X generation. A measurement campaign was conducted at the Elkem Thamshavn plant in Norway to investigate the composition of tapping gas from a silicon furnace. Over a 3-day period, the gas extracted from the tapping of the furnace was analyzed with Agilent Micro-GC, Protea atmosFIR, and Testo 350. The dust concentration in the gas was measured with a LaserDust instrument from NEO Monitors. Using the plant's existing flow and temperature measurements, mass and energy flows were calculated. Linear regressions were calculated for three predictors of NO_X formation in the taphole gas. From these calculations, the relation between total energy added to the tapping gas and NO_X showed the best correlation.

INTRODUCTION

Silicon is an important raw material for producing electronics, chemicals, and as an alloy in aluminum and other metals. The conventional way of producing silicon is by carbothermal reduction in large, submerged arc furnaces (SAF). Here, quartz is reduced to silicon according to the overall Eq. 1, where σ indicates the silicon yield of the process.

$$SiO_2 + (1+\sigma)C = \sigma Si + (1-\sigma)SiO_{(g)} + (1+\sigma)CO_{(g)} \quad (1)$$

The actual process is more complex than Eq. 1 indicates. In reality, the process involves several different reaction and furnace reaction zones, as described in detail by Schei et al.[1] A high partial pressure of SiO and temperatures over 1811 °C in the lower parts of the furnace are required to produce silicon. Figure 1 illustrates the inside of the furnace, the reactions, and how silicon and process gas go out through the taphole. The inner zone reaction can be summed up by adding the reactions, as shown in Fig. 1, where the coefficients a, b, c, and d are temperature dependent. Process gas escaping through the taphole combusts with air and is commonly called tapping gas.

As long as there is load on the furnace there will be a higher pressure inside the furnace than outside.[2] Hence, the amount of process gas escaping through the taphole depends on the over-pressure in the furnace and the pressure drop from the high temperature zone to the taphole. Usually, a matrix of SiC and SiO_2 containing slag, combined with liquid silicon limit the flow of tapping gas. Recent studies and excavations of silicon furnaces have given insight into how the furnace looks on the inside of the taphole.[3] The gas that does escape consists of CO and SiO and combusts outside the taphole, according to Eqs. 2 and 3, and is the source of several problems.

(Received April 6, 2022; accepted June 15, 2022; published online July 6, 2022)

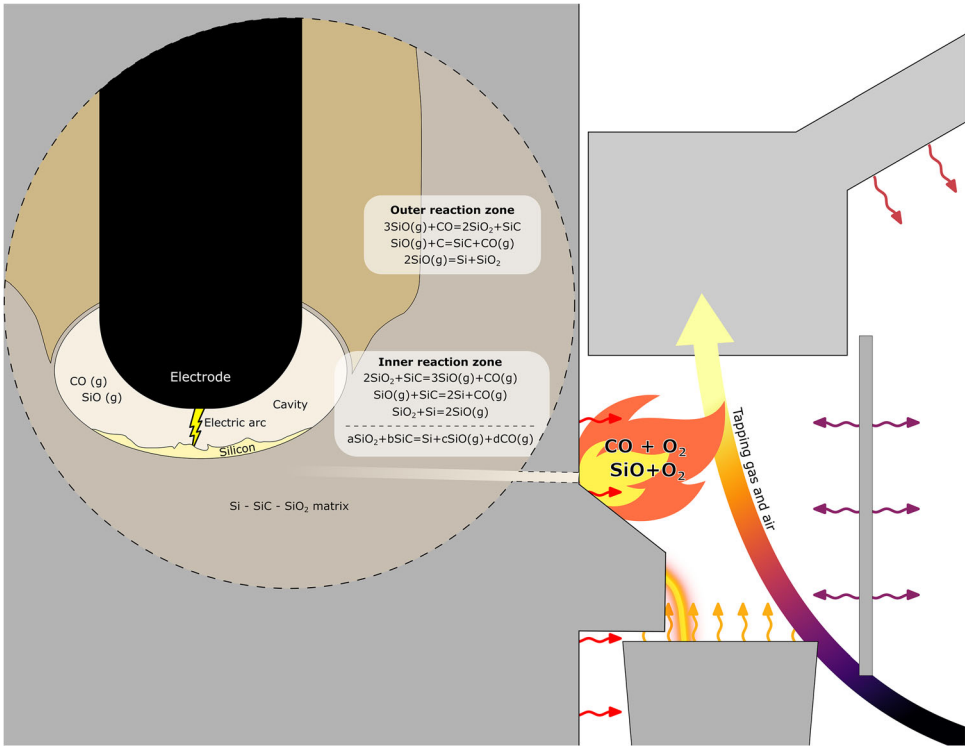

Fig. 1. Illustration of the furnace process and the tapping area where a varying amount of process gas escapes and combusts.

$$\Delta H_{500}: \ -223 \text{ Wh} \quad SiO_{(g)} + \frac{1}{2}O_{2(g)} = SiO_2 \qquad (2)$$

$$\Delta H_{500^\circ C}: \ -79 \text{ Wh} \quad CO_{(g)} + \frac{1}{2}O_{2(g)} = CO_{2(g)} \qquad (3)$$

Fine particulate amorphic silica fumes formed from burning SiO are mainly captured in dust extraction systems, but during periods of heavy gassing, a portion of the gas can leak into the furnace hall. Tveit et al.[4] summed up the different sources of PM emissions in the furnace hall, pointing to tapping as one of the big sources. Kero et al.[5] gave a broad overview of airborne emissions from silicon production.

Silica fumes have been linked to a higher risk of chronic obstructive pulmonary disease (COPD) by Johnsen[6] and recent studies of exposure to ultrafine particles[7] point to tapping operators as the most exposed group of workers. The high amount of heat released during the combustion of SiO gas is a challenge for equipment in the area and is also the source of thermal NO_X generation. NO_X emission from the silicon process is well described by Kamfjord[8] and has been modeled by Ravary et al.[9] and Panjwani et al.,[10] amongst others, where the main focus has been on the combustion of process gas occurring over the charge surface, as this is the main source of NO_X emission. Kamfjord[8] also looked at NO_X formation in tapping gas for different furnaces and found a correlation between the dust formation in the tapping gas and the NO_X formation rate, although this varied over a range from 0.03 to 0.15 kg NO per kg fume. Specialists in Elkem have also suggested a correlation between NO_X formation and the rate of energy added to the tapping gas.[11] Both correlations assume that thermal NO_X is the dominating mechanism of formation and relate the NO_X formation rate either to SiO combustion, which is strongly exothermic, or to the actual energy added to the tapping gas.

A large amount of work has also been carried out to understand the extent and composition of tapping gas. Kadkhodabeigi[12] did extensive modeling for submerged arc furnaces describing how the overpressure and metal bath level in the furnace affected tapping and gassing. A review of the different ferroalloy tapping models was done by Bublik et al.[13] and a conceptual approach to the modeling process was given by Tangstad et al.[14]

Vital to every modeling effort are data to verify the model. This paper describes a measurement campaign performed at the Elkem Thamshavn plant in Norway where the amount and composition of the tapping gas from a furnace was measured. The specific focus of the campaign was to quantify the NO_X formation and improve the understanding of how the NO_X content of the gas correlates to other gas and furnace parameters.

METHOD

The tapping gas from one of the furnaces tapped continuously at Elkem Thamshavn was measured over a period of 3 days. The furnace is a metallurgical grade silicon producing submerged arc furnace. Figure 2 shows an illustration of the tapping gas extraction system at the plant and the location of the different measurements. Note that the system usually mixes tapping gas from two furnaces during normal operation, but these were kept separate during the measurement campaign so that only tapping gas from the furnace being studied was analyzed. Flow and temperature were measured by the plant's existing systems both in the tapping channel close to the furnace, and in the smokestack after the tapping gas filter.

As the furnace rotates, tapping was done using three different tapholes during the measurement campaign. The campaign started at the end of the first taphole, measured over the whole of the second taphole and the start of the third taphole. In total the furnace rotated 68.3 degrees during the campaign. Taphole changes were done by plugging the used taphole with taphole paste, and then opening the new taphole approximately 1 h after the old taphole was plugged. New tapholes were opened by drilling in through the tapping channel and using either oxygen lances or by shooting zinc slugs from an industrial shotgun to open the last bit of the channel.

A timelapse video was taken during the measurement campaign to relate changes in the tapping gas intensity and composition to operational actions or changes. Figure 3 shows tapping at the second taphole.

For measuring the composition of the gas, the following instruments and setup were used. For the gas analysis, 3 instruments were used:

- Protea atmosFIR (FTIR instrument)
- Agilent Micro GC 490 (gas chromatograph)
- Testo 350 Portable Emission Analyzer

For gas analysis with a fast response time (120 s at 1 cm^{-1} resolution) the atmosFIR emissions monitoring FTIR system (Protea Ltd) was used.[15] The instrument and sample line are operated at a temperature of 180 °C (standard for combustion emissions). The atmosFIR runs a standard analysis model with fixed acquisition parameters and chemometric analysis for common emission gases.

An Agilent 490-PRO Micro-GC was used to quantify helium (H_2), oxygen (O_2), nitrogen (N_2), carbon dioxide (CO_2), methane (CH_4), and carbon monoxide (CO). The instrument was equipped with two separate columns and thermal conductivity detectors (TCD).[16] Channel 1 was equipped with a 10-m MS5A, RTS column. The channel was operated with Ar as the carrier gas at a pressure of 22 psi and a temperature of 110 °C. Channel 2 was equipped with a 10-m PPQ column and operated with helium carrier gas at 22 psi and a temperature of 70 °C. The inlet, injectors, and backflush module were kept at 90 °C.

Fig. 3. Tapping at the second taphole.

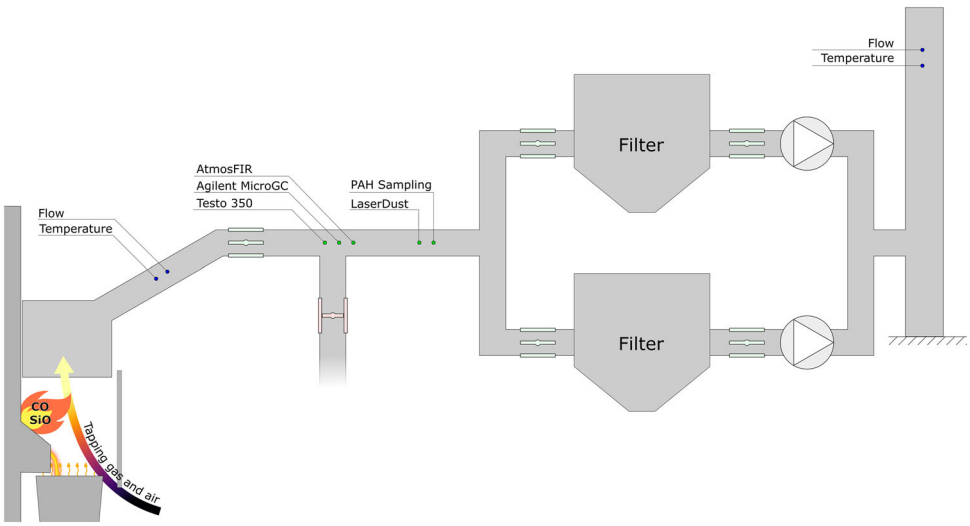

Fig. 2. Illustration of the tapping gas extraction system at the plant. New measurements are marked in green, while existing measurement systems are marked in blue (Color figure online).

Sample gas was extracted from the duct through a heated sample line with the help of a membrane pump. The total flow rate of 2.5 l/min was filtrated with a micro glass-fiber filter (0.1 μm). On the pressure side of the membrane pump the gas was split over a filter into FTIR and GC sample lines, respectively. The main flow leaves the filter house to the bypass port supplying the FTIR with a continuous sample gas flow. A small fraction of the sample flow (50 ml/min) was diverted to the GC.

Nitrogen oxide (NO_X) measurements were carried out with a Testo 350 Portable Emission Analyzer with measurements every 5 s.[17] The sensing technologies are electrochemical and infrared with response times between 10 and 40 s. The thermoelectric (Peltier-type) sample conditioner and peristaltic pump automatically remove moisture and provide a dry sample. A ceramic pre-filter was added in front of the gas sampling probe to prevent blocking because of the high particulate loading.

Measurements of the dust concentration in the tapping gas was done with a LaserDust instrument from NEO Monitors.[18]

The data were analyzed using R[19] and the figures were plotted using ggplot2.[20] Original illustrations were made with Inkscape.[21]

RESULTS AND DISCUSSION

The flow of gas through the system was measured at two points, in the smokestack after the filter and in the tapping channel close to the furnace. Figure 4 shows the flow rate measured for the two different locations. The vertical dashed lines in Figs. 4 and 8 show the time period for plugging an old taphole and opening the new one. The deviation between the flows measured in the smokestack and the tapping channel is caused by leakage of air into the tapping gas system. Air is introduced by pneumatic pulsing to clean the filter, but at least one large crack in the off-gas channel, between the measuring station and the taphole, was also observed. Hence, the flow measurement in the filter smokestack was considered the most suitable for calculating mass flows based on the gas compositions at the measuring station, since most of the dilution of process gas occurred before the measuring station. Using the flow rate in the smokestack includes dilution after the measuring station, which in turn will overestimate the calculated mass flow rates somewhat in the following section.

Temperatures for the three different positions, smokestack, measuring station, and tap channel are shown in Fig. 5. As expected, the smokestack temperature is lower than either of the other measured temperatures and it is not responsive enough to catch all the dynamics that can be seen in the other two measurements.

Dust concentrations over the entire measurement campaign are shown in Fig. 6. As seen in the figure, the LaserDust instrument was saturated at dust concentrations over 3000 mg/Nm^3. This gave some under-reporting of dust in periods with heavy gassing from the furnace. To check how correct the LaserDust measurements were, the concentrations from the LaserDust instrument were compared with an estimate of dust concentration using the reported dust production from the pneumatic senders in the filters divided by the flow through the smokestack. This is also shown in Fig. 6. Note that the pneumatic sender accumulates dust up to a given weight before sending, and the concentration is calculated by looking at the time between each send. This gives a dust concentration at a much lower resolution than the LaserDust instrument and will not show a concentration drop during the taphole changes. However, it can still be seen that the LaserDust levels are generally in the same range as the estimated concentration from the pneumatic senders, except for a few periods where the dust concentration is too high for the instrument. Averaging the LaserDust 1-s measurements over 0.5-h intervals gives a dust production very similar to the reported dust measured at the filter system. Calculating the amount of dust produced by multiplying the concentration from the LaserDust instrument and the flow through the smokestack gave a total

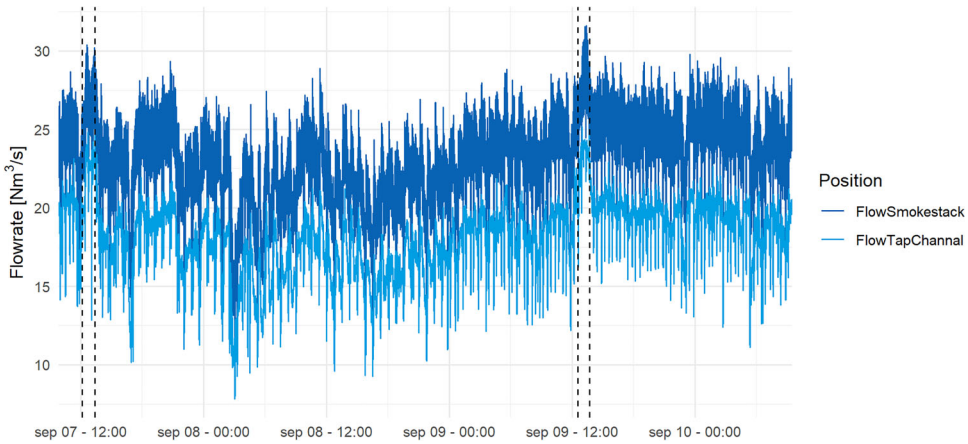

Fig. 4. Flow rate at the two measuring points in the system. The dashed vertical lines indicate the periods of changing tapholes.

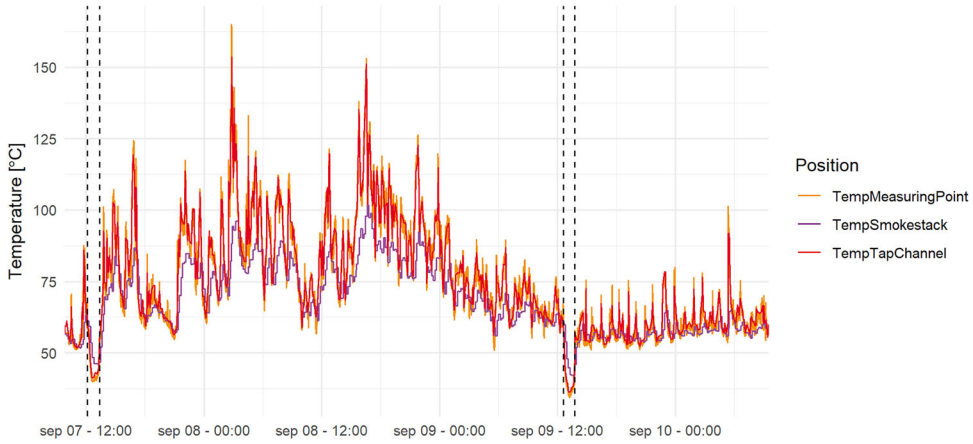

Fig. 5. Comparison of the temperature measurements in the system. The dashed vertical lines indicate the periods of changing tapholes.

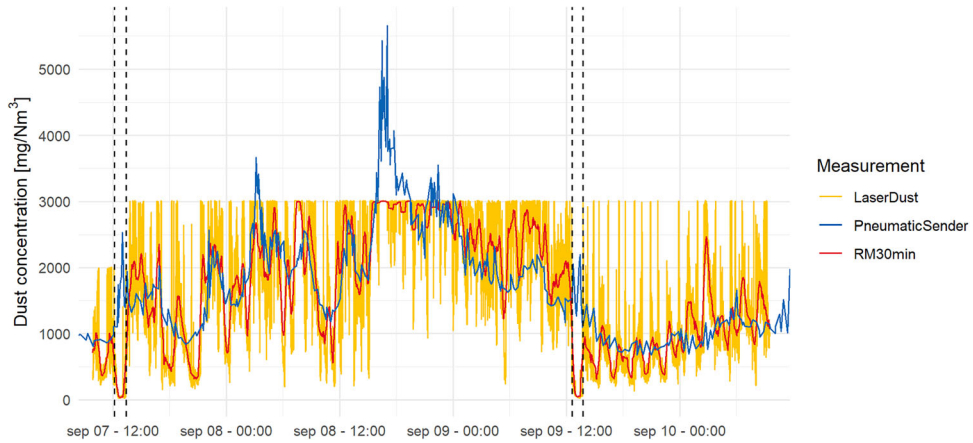

Fig. 6. Dust concentration measured by the LaserGas instrument in yellow, and an estimated dust concentration based on the dust captured in the filter divided by the gas flow through the filter in blue. The red curve is a rolling mean over 30 min for the LaserDust measurements. The dashed vertical lines indicate the periods of changing tapholes (Color figure online).

production of 9.46 MT for the period, while the reported production from the filter was 9.83 MT. This discrepancy is likely due to periods of LaserDust measurement saturation.

The CO_2 concentration measured with the different instruments is shown in Fig. 7. CO_2 concentrations from the Agilent and AtmosFir are in good agreement. The Testo 350 also measured CO_2, but concentrations of CO_2 in the tapping gas were too low for the instrument measurement range and did not give reliable results.

NO_X was measured with the Testo 350 and AtmosFIR and the results are shown in Fig. 8. Both instruments measured nitrogen oxide (NO) and nitrogen dioxide (NO_2), and NO_X was the sum of these two concentrations. As the Testo 350 instrument has a higher sampling and measurement interval it was better suited to capture the dynamic responses of the NO_X generation in the tapping gas. Especially the sharp increases in NO_X production, seen during blowing with oxygen lances, were very clearly seen in the Testo 350 measurements.

Calculating the specific NO_X per SiO_2 was done by dividing the amount of NO_X formed with the amount of SiO_2 formed over a 30-min interval, and is shown in Fig. 9. Here, the basis was the dust concentration from the LaserDust instrument, and the flow rate measured in the smokestack. NO_X concentration from the Testo 350 instrument was used and all NO_X was assumed to be in the form of NO. These values are comparable to the levels reported by Kamfjord[8] who reported an average specific NO formation of 0.076 and 0.048 kg NO/kg SiO_2 for tapping gas and furnace off-gas, respectively. During this measurement campaign, the specific NO formation for the furnace in focus was found to be lower at 0.040 and 0.029 kg NO/kg SiO_2, respectively. Looking at the total NO_X emission for

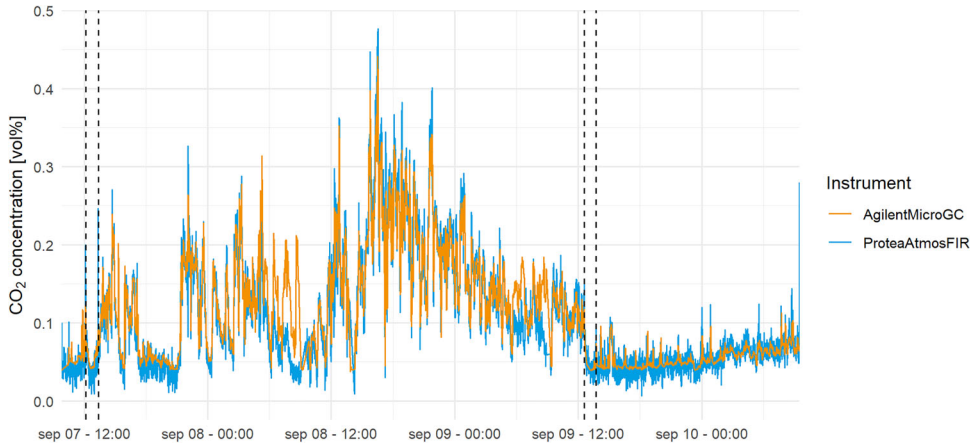

Fig. 7. CO_2 concentration measured with the Agilent Micro-GC and the Protea AtmosFIR. The dashed vertical lines indicate the periods of changing tapholes.

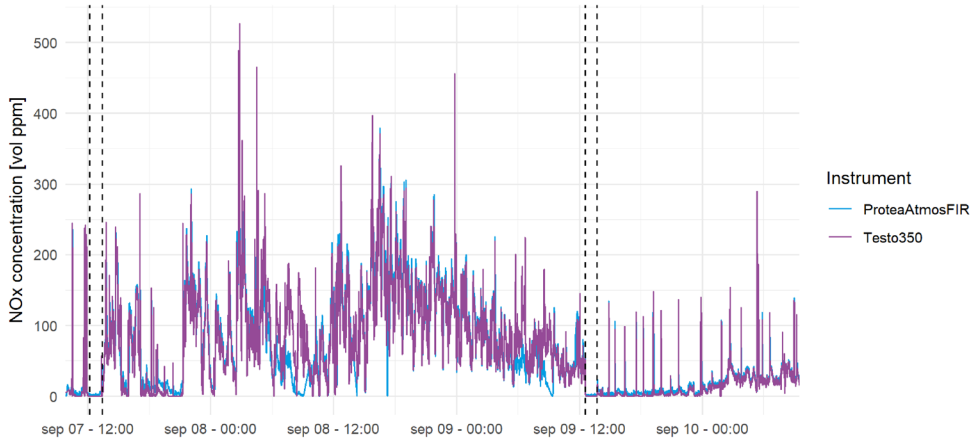

Fig. 8. NO_X concentrations in the tapping gas measured with the Testo 350 and AtmosFIR instrument. The dashed vertical lines indicate the periods of changing tapholes.

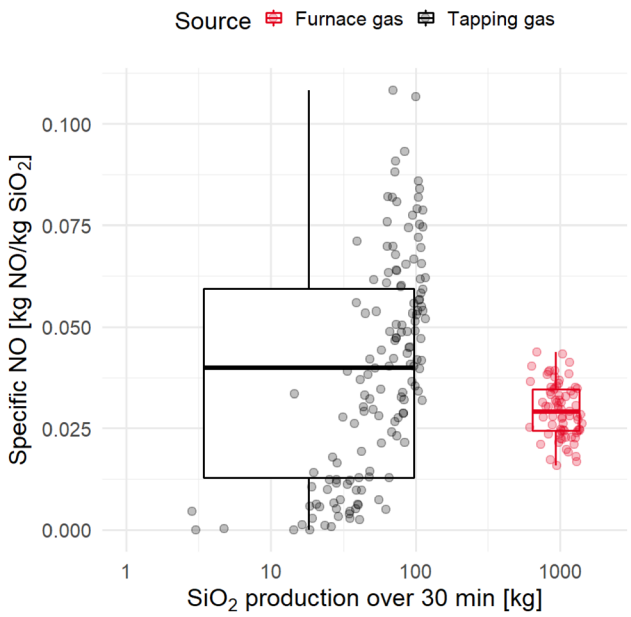

Fig. 9. Specific NO per SiO_2 for NO_X measured in the tapping gas and furnace gas.

the measurement campaign, emission from the tapping gas was 711 kg NO_X, which puts the tapping gas as contribution to the total NO_X emissions from the smelting process in the range of 5 to 20%. Note that the amounts are calculated as if all NO_X were NO_2. In practice one usually finds more NO than NO_2 in both these gasses. Distribution of NO to NO_2 was found heavily in favor of NO in the tapping gas. Figure 10 shows the ratio of NO to NO_X for the whole measurement period. Only in periods with very little NO_X measured did the distribution fall from 98–99% NO. Even though almost all NO_X is in the form of NO, emissions of NO_X are reported as NO_2 to the government. For comparative reasons, calculation of the specific NO formation was done assuming all NO_X is NO, while the total amount of NO_X emissions was calculated as NO_2.

Linear regression was done by looking at NO_X production vs temperature of the tapping gas, energy added to the tapping gas, and the SiO_2 production rate over 1-min intervals. Figure 11 shows the three linear regressions and shows that the correlation to energy added to the tapping gas

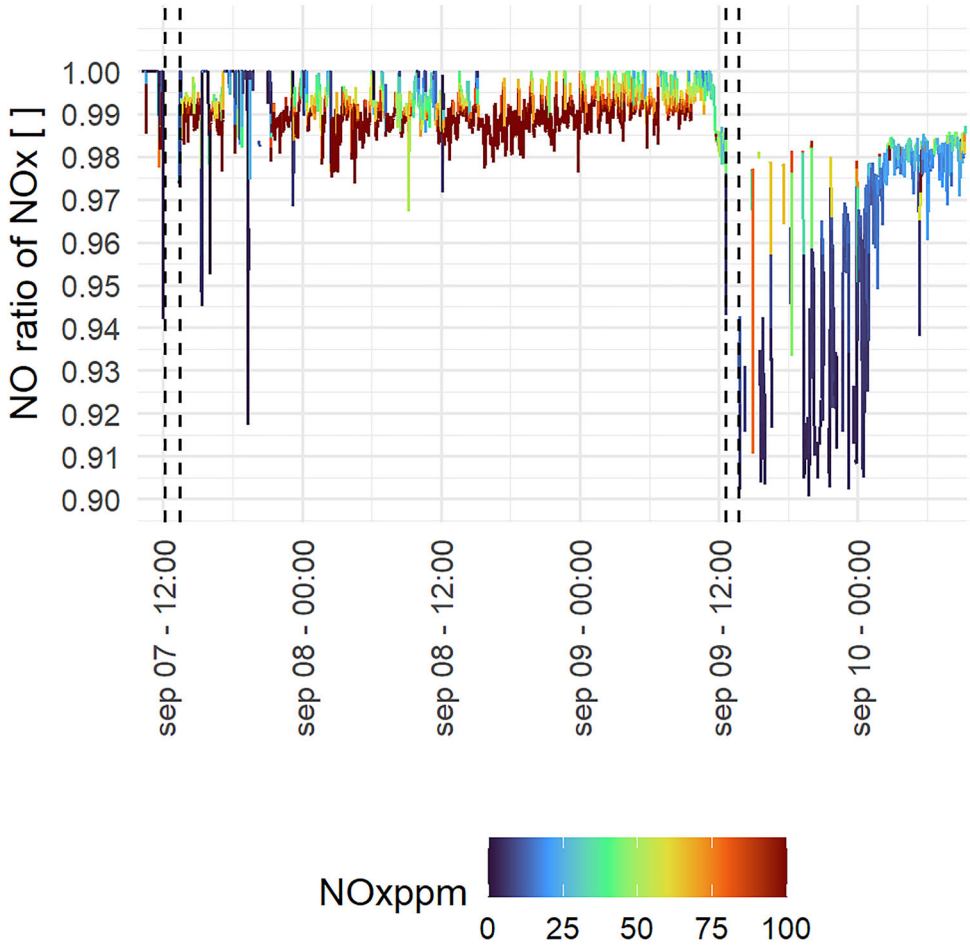

Fig. 10. Ratio of NO of NO_X as measured with the Testo 350 instrument. The color scale shows total NO_X level and illustrates that lower NO/NO_2 ratios only occur at low NO_X concentrations (Color figure online).

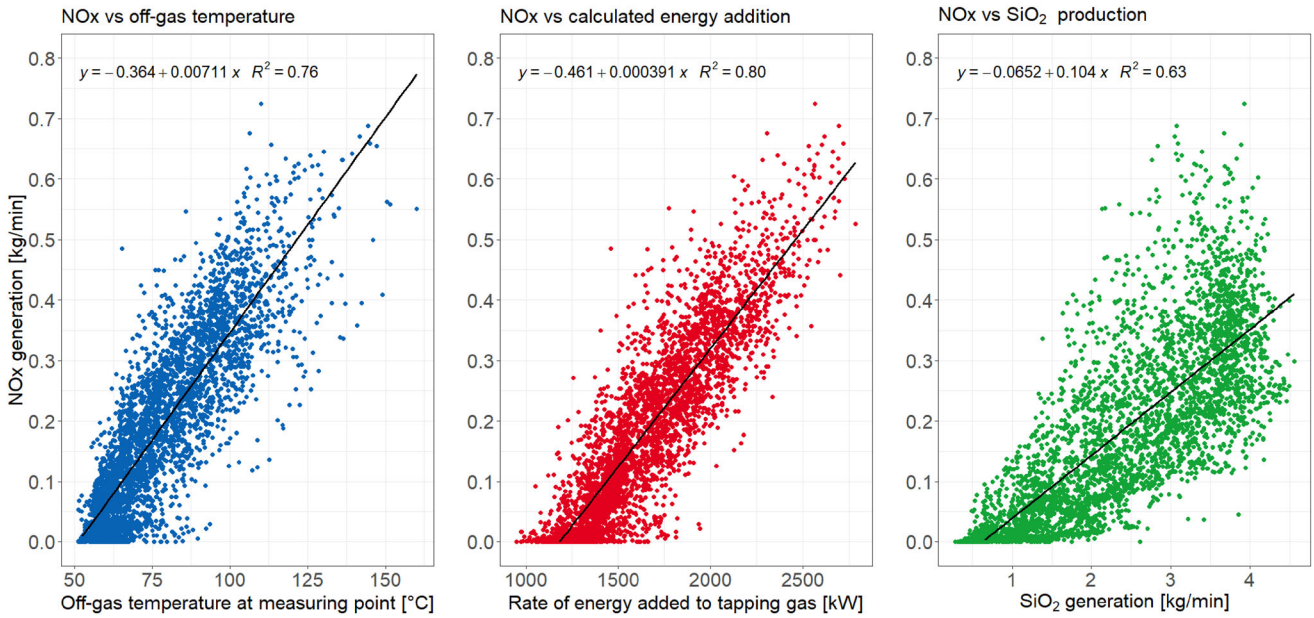

Fig. 11. Linear regression models for the top correlating parameters with NO_X generation, here NO_X weight is estimated assuming all NO_X is NO_2.

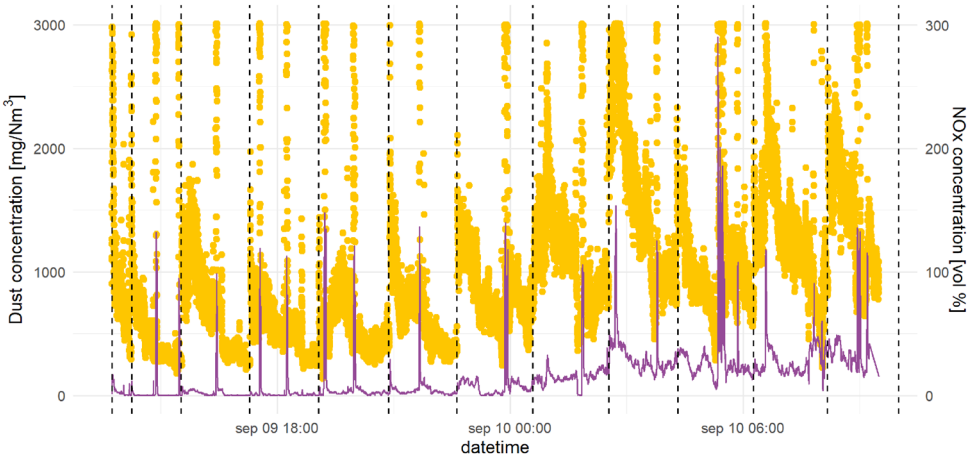

Fig. 12. Measured dust concentrations (yellow dots) and NO_X concentration (purple line) in the tapping gas during tapping on taphole 6. Dashed vertical lines indicated the start of a new tapping in an empty ladle (Color figure online).

Table I. Average values and standard deviations for added energy rate, NOx concentration, and dust concentration during the three tapholes used during the campaign, and periods of changing taphole

Taphole	Added energy rate [kW]			NO_X concentration [ppm]			Dust concentration [mg/Nm^3]		
Taphole 1	1225	+/−	151	13	+/−	37	706	+/−	450
Taphole 2	1756	+/−	335	89	+/−	62	2082	+/−	861
Taphole 3	1337	+/−	160	15	+/−	20	975	+/−	586
Change 1	900	+/−	160	0	+/−	4	165	+/−	282
Change 2	799	+/−	173	0	+/−	0	150	+/−	235

was best able to predict NO_X generation. Here the mass rate of NO_X is calculated assuming all NO_X as NO_2. Rate of energy added to the tapping gas in the smokestack is calculated by multiplying the gas flow through the smokestack with the temperature difference between the smokestack off-gas and the ambient temperature outside the smokestack, according to Eq. 4. To capture the dynamics of the tapping gas temperature changes, which partly was lost in the temperature measurement in the smokestack, the smokestack temperature was estimated by using the Testo measurement point temperature, reduced by 8.05% to match the average temperature in the smokestack. The decision to focus on the smokestack measurements, instead of the measurements in the tapping channel, was made mainly because the flow measurement in the smokestack was considered more reliable by the plant personnel.

$$P_{SS} = \dot{Q}_{SS} * (T_{SS} - T_{\text{ambient}}) * C_p \qquad (4)$$

Combustion of SiO gas is strongly exothermic and was expected to have a good correlation to the rate of NO_X formation. As Fig. 11 illustrates, both the smokestack temperature and added energy in the tapping gas seem to be a better predictor than the SiO_2 generation. This could be due to a higher accuracy in the measurements for flow and temperature than dust concentration. Saturation of the LaserDust instrument at the highest dust concentration is an obvious weakness. Another reason could be the different sources of SiO_2 generation. SiO_2 in the tapping gas is mainly formed by SiO escaping the taphole, but a portion is also formed during blowing with oxygen in the taphole, where Si is oxidized. Some SiO will also form from oxidizing Si in the ladle during refining and directly from the metal stream. These different oxidization mechanisms could occur at conditions that favor NO_X formation differently, giving a different NO_X to SiO_2 correlation. Figure 12 shows the measured dust concentration and NO_X concentration during tapping at the third taphole, with dashed lines indicating the start of tapping on a new ladle. Here it can be seen that the dust concentration generally increases once a tapping starts at a new ladle, but the NO_X concentration does not necessarily increase. During tapping, there are several peaks in both NO_X and dust concentration which coincide with blowing oxygen in the taphole. Increased SiO_2 generation from the ladle and metal stream is expected during the start of each tap as more of the metal bath is exposed and the stirring in the ladle is more violent. The lack of increased NO_X concentrations in these periods indicate that the

SiO_2 formation in the ladle and metal stream does not increase NO_X formation the same way as seen with blowing oxygen in the taphole.

There were significant differences in the intensity of gassing for the three different tapholes used during the measurement campaign. Table I shows the average values and standard deviation of the added energy rate to the tapping gas, NO_X concentration, and dust concentration for all three tapholes used as well as the periods of taphole change. Although this work does not investigate which factors cause the variation in tapping gas intensity, it is still worth noting how large the difference can be from one taphole to the next. Good tapping conditions are certainly a prerequisite for good furnace operation.

CONCLUSION

The tapping gas of a large silicon-producing furnace was measured and analyzed over a 3-day period. Measurements show that the amount of tapping gas varied by factors up to 10, using the amount of CO_2 and dust in in the tapping gas as indicators of the amount of gassing. CO_2 concentrations were found to be in the range of 380 ppm up to short peaks over 4500 ppm. Similarly, the dust concentrations were found to be in a range from 200 mg/Nm^3 to over 5000 mg/Nm^3. This corresponds to a tapping gas velocity up to approximately 25 Nm/s out of the taphole, assuming the taphole has a diameter of 75 mm, which corresponds well with the assumptions and calculations of Kadkhodabeigi.[12]

NO_X concentrations in the tapping gas were measured to be in the range of 0 to 500 vol ppm. During the almost 3-day measurement campaign, a total of 711 kg NO_X, re-calculated as NO_2 from NO and NO_2 measurements, was produced, which averages to a production rate of 10 kg NO_2/h. This NO_X production puts the NO_X contribution from tapping gas in the size range of 5–20% of the total NO_X generation from the smelting process. Measured NO_X consisted generally of over 98% NO and the rest was NO_2. The specific kg NO/kg SiO_2 ratio was found to be lower, but in the same range as previously reported values by Kamfjord.[8]

Linear regression modeling showed that NO_X was best correlated with the added energy in the tapping gas, rather than the dust concentration in the tapping gas. An important factor for correlating NO_X to added energy was using a temperature measurement fast enough to capture the dynamics of the tapping gas.

ACKNOWLEDGEMENTS

This work was funded by the research center FME HighEFF (257632) and the Controlled Tapping Project (267621). Extensive support and help were provided by the team at Elkem Thamshavn, both in terms of planning and carrying out the campaign, installing equipment, and providing data. The authors gratefully acknowledge the help from Elkem Thamshavn and the financial support from the Research Council of Norway and the user partners in the involved centers and projects.

FUNDING

Open access funding provided by NTNU Norwegian University of Science and Technology (incl St. Olavs Hospital - Trondheim University Hospital).

CONFLICT OF INTEREST

The authors declare that they have no conflicts of interest.

OPEN ACCESS

REFERENCES

1. A. Schei, J.K. Tuset, and H. Tveit, *Production of high silicon alloys*. Trondheim: TAPIR (1998).
2. H. Tveit, T. Halland, K.-I. Landrø, S. Tore, and B. Ravary, *The Tapping Process in Silicon Production., Silicon for the Chemical Industry VI*, Trondheim, Norway (2002).
3. M. Tangstad and M. Folstad, *Proceedings of the 16th International Ferro-Alloys Congress* (INFACON XVI) 2021, Sep. 2021. doi: https://doi.org/10.2139/ssrn.3922187.
4. H. Tveit, V. Andersen, K.H. Berget, and R. Jensen, *The tapping process in silicon production*, Furnace Tapping Conference, Muldersdrift, South Africa (2014).
5. I. Kero, S. Grådahl, and G. Tranell, *JOM* 69(2), 365 https://doi.org/10.1007/s11837-016-2149-x (2017).
6. H.L. Johnsen, *Lung function, respiratory symptoms, and occupational exposure: A five-year prospective study among employees in Norwegian smelters*, 2009, Accessed: Mar. 28, 2022. [Online] https://www.duo.uio.no/handle/10852/28133.
7. R.B. Jørgensen, I.T. Kero, A. Blom, E.E. Grove, and K.H. Svendsen, *Nanomaterials* 10(12), 2546 https://doi.org/10.3390/nano10122546 (2020).
8. N.E. Kamfjord, *Mass and Energy Balances of the Silicon Process*, PhD Thesis, NTNU, Trondheim, Norway, 2012.
9. B. Ravary, C. Colomb, and S.T. Johansen, *Proceedings of the 11th International Ferro-Alloys Congress (INFACON XI)* (2007), pp. 499–506.
10. B. Panjwani and J.E. Olsen, *Combustion and mechanism of NOx formation in Ferrosilicon*, European Combustion Meeting, Jun. 2013.
11. K.H. Berget, private communication. Mar. 2021.

12. M. Kadkhodabeigi, *Modeling of Tapping Processes in Submerged Arc Furnaces*, PhD Thesis, NTNU, Trondheim, Norway (2011).
13. S. Bublik, J.E. Olsen, V. Loomba, Q.G. Reynolds, and K.E. Einarsrud, *Metall. Mater. Trans. B* 52, 2038. https://doi.org/10.1007/s11663-021-02134-5 (2021).
14. M. Tangstad, E. Ringdalen, J.E. Olsen, K.E. Einarsrud, E. Myrhaug, and Q. Reynolds, *Conceptual Model Of Tapping Mechanisms In FeSi/Si Furnaces*, Proceedings of the 16th International Ferro-Alloys Congress (INFACON XVI) 2021, Sep. 2021 https://doi.org/10.2139/ssrn.3922189.
15. atmosFIR - Analyser Product Range | Protea Ltd https://www.protea.ltd.uk/atmosfir. Accessed Mar. 31, 2022.
16. 490-PRO Micro GC System | Agilent https://www.agilent.com/en/product/gas-chromatography/gc-systems/490-pro-micro-gc-system. Accessed Mar. 31, 2022.
17. Testo 350 - Control Unit for flue gas analysis system | Testo Ltd https://www.testo.com/en-UK/testo-350/p/0632-3511. Accessed Mar. 31, 2022.
18. LaserDust™ – Neo Monitors https://neomonitors.com/product/laserdust/. Accessed Mar. 31, 2022.
19. R Core Team, *R: A Language and Environment for Statistical Computing*. Vienna, Austria: R Foundation for Statistical Computing, 2020. [Online] https://www.R-project.org/.
20. H. Wickham, ggplot2. *Springer, New York,* https://doi.org/10.1007/978-0-387-98141-3 (2009).
21. Inkscape Project, *Inkscape*. 2022. [Online] https://inkscape.org.